Available online at www.sciencedirect.com
ScienceDirect
Journal of Sound and Vibration 318 (2008) 527–548
JOURNAL OF SOUND AND VIBRATION
www.elsevier.com/locate/jsvi

Self-modulation of acoustic waves in resonant bars

L. Fillinger[a,*], V.Yu. Zaitsev[b], V.E. Gusev[c], B. Castagnède[a]

[a]*Laboratoire d'Acoustique de l'Université du Maine, 72085 Le Mans cedex 9, France*
[b]*Institute of Applied Physics, Russian Academy of Sciences RAS, Nizhny Novgorod 603950, Russia*
[c]*Laboratoire de Physique de l'État Condensé, 72085 Le Mans cedex 9, France*

Received 18 October 2006; received in revised form 8 February 2008; accepted 13 February 2008
Handling Editor: C. Morfey
Available online 8 August 2008

Abstract

Observations of the induced transparency in the oscillations of a glass bar containing an ''artificial crack'' in the form of a saw-cut with a tightly inserted small metal plate are reported. In such a configuration, the increase of the resonator quality factor with increasing wave amplitude (denoting a decrease of dissipation which will be referred to as *self-induced transparency*) has been observed indicating an important role of the amplitude-dependent losses introduced by the inter-surface contacts. The self-induced transparency manifests itself also by the discontinuities (jumps) in the acoustic wave amplitude measured as a function of sweeping excitation frequency around the sample eigenfrequencies and by a self-modulation instability of the primary acoustic wave. This instability leads to the generation of side-lobes in the wave spectrum near the fundamental excitation frequency. The developed theoretical model confirms that all these observations can be self-consistently attributed to nonlinearity of the sound dissipation process. Possible physical mechanisms of the nonlinear dissipation are discussed. Although self-modulation has already been observed in nonlinear acoustical systems, to the knowledge of the authors, the reported data constitute the first observation of the instabilities due to essentially dissipative system behaviour that requires neither nonlinear elasticity nor multimode interaction.

1. Introduction

In classical nonlinear acoustics of fluids and perfect crystals nonlinear phenomena are commonly attributed to elastic (non-dissipative) nonlinearity of the material. Its origin is associated with weak anharmonicity of the inter-atomic potential and the so-called geometrical nonlinearity (the $(\vec{v}\cdot\nabla)\vec{v}$ term in the Euler equation or quadratic terms in the relation between strains and displacement gradients in the Lagrange variables) [1]. In ''non-classical'' nonlinear acoustics of micro-inhomogeneous solids, the nonlinear phenomena are conventionally attributed to the so-called hysteretic nonlinearity [2], which contains both elastic and dissipative parts. These observations of nonlinear elasticity have lead to applications in non-destructive testing/evaluation as reported in the review articles [3,4]. There is also increasing number of the experiments indicating an important role of other dissipative mechanisms of nonlinearity [5,6], which are not related to

*Corresponding author.
E-mail address: laurent.fillinger@univ-lemans.fr (L. Fillinger).

0022-460X/$ - see front matter © 2008 Published by Elsevier Ltd.
doi:10.1016/j.jsv.2008.02.034

hysteretic phenomena caused by microfriction and/or adhesion at microstructural defects in the material. It is important that in the case of dissipative nonlinearities, both a regime of induced absorption (when the absorption increases with increasing wave amplitude) and of induced transparency (when the absorption diminishes with increasing wave amplitude) are possible [7]. We report *observations* of the regime of the induced transparency in the oscillations of a glass bar containing an "artificial crack" in the form of a saw-cut with a tightly inserted small metal plate. In such a configuration, the increase in the resonator quality factor with increasing wave amplitude was observed, which indicated an important role of the introduced inter-surface contacts in the documented phenomena. The self-induced transparency manifests itself also by discontinuities (jumps) in the acoustic wave amplitude measured as a function of sweeping excitation frequency (i.e., discontinuities in the resonance curve) and by self-modulation of acoustic wave, leading to the generation of the side-lobes in the wave spectrum near the fundamental excitation frequency. The developed theoretical model confirms that all these observations can be self-consistently attributed to nonlinearity of the sound dissipation process. Possible physical mechanisms of the nonlinear dissipation are discussed. From the general physics point of view the reported observations contribute to increasing volume of experimental and theoretical evidence of the spatiotemporal patterns formation via the development of instabilities in systems driven away from equilibrium [8]. Indeed, the present paper shows that instabilities can develop in the presence of suddenly decreasing positive dissipation, without the need of multi-component excitation [9], multimode interaction [10], nonlinear elasticity or genuine negative dissipation [11].

2. Experimental set-up and observations

The experiments were carried on a set-up that allowed for simple comparison between two states of the same sample, either with or without a crack-like defect. The idea was to use a "removable defect" in order to get different configurations of the sample which differ only by the presence or absence of the defect. To simplify the interpretation of the influence of the defect, we chose a well known geometry of the sample in the form of a rod subjected to longitudinal excitation (see Fig. 1). It was made of glass with dimensions of about 20 cm in length and 1 cm in diameter. The rod was cemented via an intermediate piezoelectric disk-actuator onto a heavy backload in order to produce a nearly acoustically rigid boundary condition. At the other end of the rod, a light accelerometer was glued, so that this boundary could be considered as acoustically free. At a distance of 1.5 cm from the rigid boundary (that is in the region of near-maximal strain for the lower eigenmodes) a saw-cut of 1 mm thickness and several mm depth was made, in which a small metal plate could be inserted in order to create an artificial crack-like defect. Conditioning amplifier, analyser, generator and power amplifier allowed for acquiring resonance curves, vibration spectra and temporal waveforms. For the

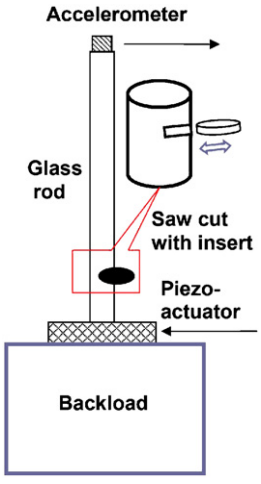

Fig. 1. Experimental set-up constituted of a 1D rod-shape resonator with one rigid and the other acoustically free boundary. The glass rod had a saw-cut in which a metallic plate could be inserted to create a crack-like defect.

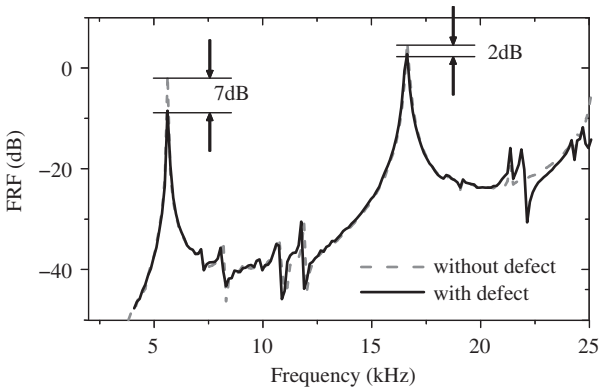

Fig. 2. Frequency response function for the sample with and without defect indicating that the defect influence is mostly dissipative, which is clearly visible near the resonance maxima.

chosen dimensions of the sample, its several lower-order modes can be modelled with a good accuracy in the framework of 1D approximation.

Preliminary measurements were performed on the sample in the absence of the defect. The obtained spectrum of resonance frequencies confirmed the validity of the 1D model with one rigid and the other free boundary conditions (see the dashed curve in Fig. 2): the ratios of the resonance frequencies to the first one were close to odd integers. Acquisition of resonance curves with different levels of driving amplitude showed that the defect-free sample was linear in the whole achievable range of excitation, that is up to strain of the order of 10^{-6}.

The presence of the metal plate in the saw-cut introduces contacting interfaces into the sample. As real macroscopic surfaces are not perfectly flat, the contact area between the glass rod and the metal plate is smaller than what is apparent [12], there is an ensemble of non-conformal contacts whose number and area may change with the applied load. Non-conformal contacts are known to exhibit nonlinearities in their elastic [12] and dissipative [7,13] behaviour. Such a nonlinear response is likely to affect the characteristics of resonance curves. In the first approximation, nonlinear elasticity will influence the resonance frequencies, while nonlinear dissipation will mostly manifest itself in the change of resonance amplitudes and quality factors Q. Fig. 2 represents the frequency response function of the sample (FRF, i.e., the vibration spectrum divided by the spectrum of the excitation). The solid curve is obtained in the presence of the defect at a moderate excitation amplitude. It almost coincides with the dashed curve corresponding to the defect-free configuration, showing the weak influence of the defect far from resonance frequencies. The most noticeable manifestation of the defect is visible near the resonances in the form of lowering the resonance amplitudes. This variation in the FRF amplitude at the resonances can be conveniently used for tracking the resonance-peak Q-factor as a function of the excitation amplitude. Indeed, the amplitude at a resonance is proportional to Q. Although for a linear oscillator, the Q-factor can be equivalently determined via the resonance width, this method becomes ambiguous when the resonance curves are nonlinearly distorted and exhibit jumps as in the examples shown in Fig. 3. However, even in such a case, using the Q-factor initially determined via the resonance width in the linear small-amplitude regime and measuring the FRF amplitude at the resonance at higher amplitudes, one can unambiguously evaluate the current value of the Q-factor in the nonlinear regime as well. Therefore, the strong variation in the FRF amplitude clearly indicates pronounced modification of the overall dissipation in the sample at different excitation amplitudes. In contrast, for a linear oscillator all FRF-curves should be identical for all excitation amplitudes. Another remarkable feature revealed in the experiments was that the resonance frequencies were kept almost unchanged: the nonlinear influence of the defect in many cases was mostly restricted to modification of the dissipative characteristics of the sample. Measurements performed with varying excitation amplitude show more clearly this tendency. Fig. 3 presents several FRF-curves measured around the second mode and obtained in a rather wide amplitude range. The remarkable feature of these curves is that the frequency shift is hardly noticeable (much less than the resonance curve width), whereas the FRF amplitudes and thus the resonance Q-factor exhibits strong increase (up to 1.8

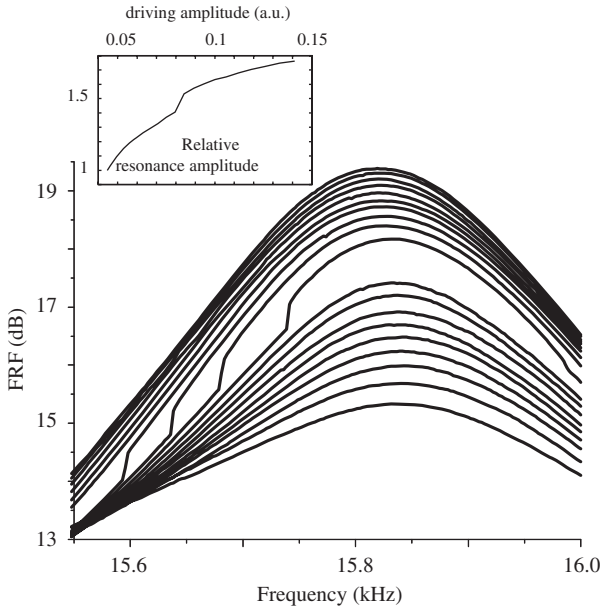

Fig. 3. Successive FRF-curves obtained with 0.5 dB steps in excitation amplitude. For 9 dB increase in the excitation amplitude the FRF-maximum value increases with uneven rate over 4 dB in total (corresponding to strain increase from about 6.2×10^{-7} to 2.8×10^{-6}). Inset shows the relative evolution of resonance amplitude with driving amplitude.

times, see the evolution of the FRF-maximum amplitude in the inset). On such a plot, FRF-curves for a linear system would coincide and inset would present horizontal line. Here, in contrast, the higher is the excitation level, the higher is the curve, thus manifesting that the acoustic loss decreases with increasing amplitude. For convenience, we will call this behaviour *induced transparency*. The term "induced" means that it is controlled by the amplitude (i.e., it is nonlinear) and "transparency" means that the dissipation decreases, the medium becomes less opaque. An interesting feature of several of these curves is the appearance of *jumps*, consisting in sudden increase of the FRF amplitude with only slight change in the driving frequency. These jumps indicate existence of some instability (or bistability) in the system. Another phenomenon typical of these samples was the effect of self-modulation observed in the vicinity of the resonance frequencies for sinusoidal excitation exceeding a certain threshold. This modulational instability manifests itself in slow (on the scale of the driving frequency) *periodic* modulation of the envelope of the oscillations. The period of this modulation vary with the driving frequency and with the excitation amplitude and could almost tend to infinity (that is to near-zero modulation frequency). The modulation could have a complicated shape and could be rather deep as shown in the upper part of Fig. 4 (obtained close to the resonance frequency of the fourth mode, which exhibited a behaviour similar to that of the second mode). The spectrum of this signal (shown in the bottom of Fig. 4) indicates that the modulation appears as broadening of the peaks corresponding to the harmonics of the driving frequency but without existence of subharmonics (the modulation side-lobes are resolved in the inset).

3. Mathematical modelling

Various models are known that reproduce effects like jumps and modulation instability. For instance, the Duffing oscillator exhibits bistability that manifests itself by jumps on experimentally acquired resonance curves [11]. This effect is caused by the nonlinear elasticity and is accompanied by a variation in the resonance frequency. According to the results of our experiments, we can neglect nonlinear elasticity in modelling, since the nonlinear resonance shifts were negligible compared to the resonance-curve width variations. In strongly nonlinear media, a monochromatic driving can excite subharmonics or frequency pairs whose sum equals to the driving frequency. Signals of this type are characterised by a modulation of the temporal waveforms and

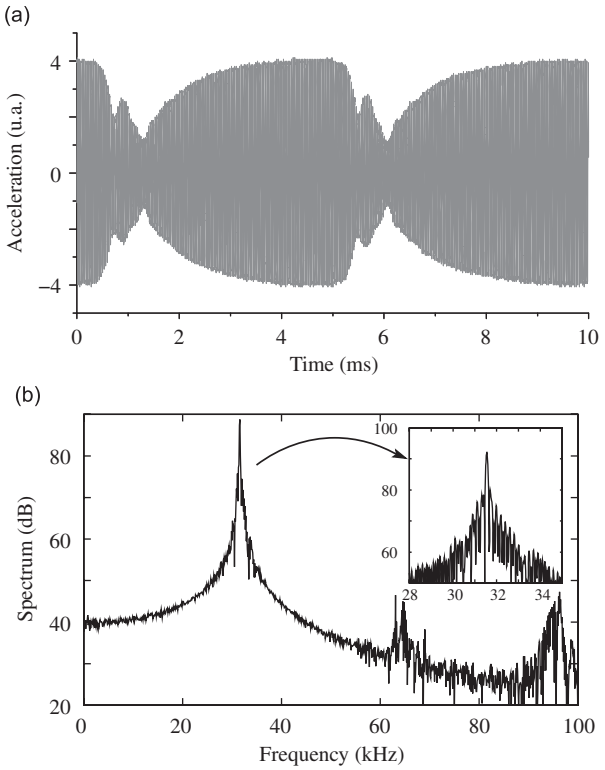

Fig. 4. Example of temporal acoustic envelope waveform (a) with well developed self-modulation and its associated spectrum (b). The inset shows the main peak with a resolution that makes sidebands visible.

by the presence of frequency components significantly lower than the driving frequency in the spectrum [10]. We did not observe such frequency components. Another system that demonstrates a behaviour similar to modulation instability is the Van der Pol autonomous oscillator [11] with an additional external excitation. The autonomous oscillator is self-exciting since it exhibits nonlinear dissipation that is negative at low amplitude and becomes positive above a threshold. Additional external excitation at a frequency close to that of the self-oscillations may either synchronise the oscillator or induce a regime of modulated oscillations. Our experiments manifested, however, that the nonlinear dissipation due to the defect always remained positive, although it could decrease with the excitation amplitude. Since the already documented models accounting for self-modulation cannot be directly applied to our experiments, we have developed a model based on the observations of the linear behaviour in the defect-free sample and the essentially nonlinear-dissipative influence of the defect.

Thus no nonlinear elasticity was introduced in the model in the form of a 1D resonator of length L which is driven at $x = 0$ by a sinusoidal displacement of amplitude A_0 at angular frequency ω. Boundary $x = L$ of the resonator is free. The displacement field U of the resonator is then described by the following equations :

$$\begin{cases} U_{tt} - c_0^2 U_{xx} - \hat{D}(U_{xxt}, U_{xt}) = 0, \\ U(x = 0, t) = A_0 \cos(\omega, t) \\ U_x(x = L, t) = 0, \end{cases} \tag{1}$$

where indices t and x denote time and space derivatives, respectively, c_0 is the linear sound speed in the material. $\hat{D}$ is the dissipation operator that takes the conventional form $\alpha_1 U_{xxt}$ in the linear case, where α_1 is the linear viscosity coefficient. Introducing the variable $V = U - A_0 \cos(\omega t)$ one may get equivalent equations

with zero boundary conditions, but with a source in the right-hand side of the wave equation:

$$\begin{cases} V_{tt} - c_0^2 V_{xx} - \hat{D}(V_{xxt}, V_{xt}) = A_0\omega^2 \cos(\omega t), \\ V(x=0,t) = 0, \\ V_x(x=L,t) = 0. \end{cases} \tag{2}$$

The advantage of this formulation is that the eigenmodes of the associated conservative linear system are known. They have the form $\Phi_n(x) = \sin(k_n x)$ with wavenumbers $k_n = (2n-1)\pi/(2L)$, where $n = 1, 2, 3, \ldots$ are the mode numbers. Each mode corresponds to angular frequency $\omega_n = c_0 k_n$. Arbitrary displacement V can be represented via the basis of the eigenmodes: $V = \sum_n V_n(t)\Phi_n(x)$, where V_n is the amplitude of the nth mode. For a sinusoidal excitation close to a resonance frequency, mostly the mode associated with that frequency will be excited, so that the system reduces to a single oscillator.

Let us now consider a dissipation operator of the form:

$$\hat{D}(V_{xxt}, V_{xt}) = [\alpha_1 + \alpha_2 f(V_{xt})\delta(x - x_{\mathrm{cr}})]V_{xxt}. \tag{3}$$

The first term represents the linear non-localised dissipation (background dissipation), whereas the second term accounts for the presence of the localised defect and thus contains a Dirac delta-function $\delta(x - x_{\mathrm{cr}})$. Factor $f(V_{xt})$ describes the nonlinear dissipation at the defect. The dissipation function f is supposed to tend to a constant at low amplitude in order to describe a nearly linear behaviour of the resonator at lower amplitudes, $f(0) = 1, f'(0) = 0$. Further, the Taylor expansion of the dissipation function f should not contain a linear term, and its lowest non-constant term should be quadratic. Thus function f is even in the first approximation, and we will see later that only its even part contributes to the dynamics of the system in the first approximation. Under such assumptions, at low amplitudes the dissipation operator (3) reduces to $(\alpha_1 + \alpha_2\delta(x - x_{\mathrm{cr}}))V_{xxt}$, which corresponds to a linear (though partially localised) dissipation. We are interested in modelling the induced transparency, which means that the dissipation function should be decreasing in a certain range of oscillation amplitudes. Furthermore, it should remain positive to be physically relevant to the experiments. The argument of this dissipation function is chosen to be the strain rate V_{xt}. Note that the location of the defect with respect to the strain- or displacement distribution quantitatively modifies its influence on the dissipation in the system, the result of which also depends on a particular model of the nonlinear dissipation operator (involving displacements, their gradients or rates). For example, one may assume that the nonlinear dissipation can be rather a function of strain than the strain rate. One or another choice of the dissipation operator would change the details and modify quantitative factors, but the main qualitative conclusions on the system behaviour, which are obtained below using the operator described by Eq. (3), will remain valid. In particular, the conclusion on the self-modulation characteristic frequencies will remain valid, since we consider the system behaviour in a narrow frequency range near a particular resonance.

We shall now obtain simpler equations describing the nonlinear system. Substituting the modal decomposition of the displacement field into Eq. (2) and singling out the nth mode, the frequency of which is close to the driving frequency, one obtains approximately:

$$(V_{n,tt} + \alpha_1 k_n^2 V_{n,t} + c_0^2 k_n^2 V_n)\frac{L}{2} + \alpha_2 V_{n,t} k_n^2 \Phi_n^2(x_{\mathrm{cr}}) f(V_{n,t}\Phi_n'(x_{\mathrm{cr}})) = \frac{A_0\omega^2 \cos(\omega t)}{k_n}. \tag{4}$$

A more accurate equation would involve summation over the modes in the dissipation term. However, we retain there only the nearly resonant nth mode, which means that we consider only the self-action of the mode, bearing in mind that other modes give negligibly small contributions to the total displacement field, which is consistent with the experimental observations. The system now reduces to the equation of an oscillator. For further consideration, it will be convenient to use non-dimensional variables. We will use the normalised time $\tau = \omega_n t$ and variable $S = k_n V_n$ corresponding to the strain component of the excited mode. Then the oscillator equation can be rewritten as

$$S_{\tau\tau} + \frac{1}{Q(S_\tau)} S_\tau + S = 2F \cos(\nu\tau) \tag{5}$$

with

$$\frac{1}{Q(S_\tau)} = \frac{1}{Q_1} + \frac{f(\omega_n S_\tau \cos(k_n x_{cr}))\,\sin(k_n x_{cr})^2}{Q_2}, \tag{6}$$

where $v = \omega/\omega_n \approx 1$ is the normalised driving frequency, $F = A_0 v^2/L$ is the normalised driving amplitude. $Q_1 = c_0/(\alpha_1 k_n)$ is the quality factor that the mode would have in the absence of the defect, and $Q_2 = Lc_0/(2\alpha_2 k_n)$ is its minimal value considering only the loss at the defect. By assumption, the dissipation function can be replaced by 1 at low amplitude. The low-amplitude quality factor Q_0 of the mode is then given by

$$Q_0 = Q_1 \frac{1}{1 + (Q_1/Q_2)\sin^2(k_n x_{cr})}. \tag{7}$$

As the observed modulation was slow on the scale of the driving frequency, it is natural to use the slowly varying amplitude technique. We search a solution in the form $S = a\cos(v\tau + \varphi)$, where a and φ are the slowly varying amplitude and phase. The derivative of S over τ involves the derivatives of a and φ which are small parameters of the order of $\mu \ll 1$. When applying the slowly varying amplitude technique, a first-order approximation should keep only terms of the order of μ. The terms of the order of μ^2 (involving two derivatives of a or φ over τ) in $S_{\tau\tau}$ will be neglected, and $S_{\tau\tau}$ can be approximated as $S_{\tau\tau} \approx -(v^2 + 2v\varphi_\tau)a\cos(v\tau + \varphi) - 2va_\tau \sin(v\tau + \varphi)$. We are interested in resonant behaviour, which assumes sufficiently small dissipation: the resultant quality factor is high (of the order of μ^{-1}) and only zeroth-order approximation of S_τ should be substituted in the dissipation term. At zeroth order, derivative $S_\tau \approx -va\sin(v\tau + \varphi)$ contains only a v component. But the nonlinearity of the dissipation function will produce harmonics of the driving frequency. Further we should only keep the terms at frequency v (harmonic balance), so that the dissipation term should be approximated as $S_\tau/Q(S_\tau) \approx \Gamma_1 \cos(v\tau + \varphi) + \Gamma_2 \sin(v\tau + \varphi)$. Coefficients Γ_i are obtained by projection of the dissipation term on the relevant Fourier component. For instance:

$$\Gamma_2 = \frac{\int_0^{2\pi/v} (S_\tau/Q(S_\tau))\sin(v\tau + \varphi)\mathrm{d}\tau}{\int_0^{2\pi/v} \sin^2(v\tau + \varphi)\mathrm{d}\tau} = -\frac{av\tilde{f}(a)}{Q_0} \tag{8}$$

and Γ_1 is obtained by substituting the sin by cos. However, the contribution related to Γ_1 is only a small correction to the term containing Γ_2 and can be neglected. Furthermore, only the even part of the dissipation function contributes to the expression of Γ_2, while Γ_1 is a function of its odd part. Since the odd part of the dissipation function does not contribute to the period-averaged dynamics of the system, therefore in the first-order approximation it was not introduced in the model. Notation $\tilde{f}(a)$ is introduced for convenience, and it will be referred to as the averaged dissipation function.

Using the identity $\cos(v\tau) = \cos(v\tau + \varphi)\cos(\varphi) + \sin(v\tau + \varphi)\sin(\varphi)$, the source term of Eq. (5) can be decomposed into two quadrature components. Substitution of this decomposition into Eq. (5) and combining coefficients at independent components $\cos(v\tau + \varphi)$ and $\sin(v\tau + \varphi)$ yield the following equations for the amplitude a and the phase φ:

$$\begin{cases} a(1 - v^2) - 2av\varphi_\tau = 2F\cos(\varphi), \\ -2va_\tau - av\tilde{f}(a)/Q_0 = 2F\sin(\varphi). \end{cases} \tag{9}$$

This system can be simplified taking into account that the excitation frequency v is close to that of the considered mode ($v \approx 1$): $1 - v^2 = (1 - v)(1 + v) \approx -2v\Delta v$, where the normalised detuning from the resonance frequency $\Delta v = v - 1 \sim O(\mu)$ is also a small parameter. This finally leads to the approximate dynamical equations for the mode, which will be analysed as follows:

$$\begin{cases} a\Delta v + a\varphi_\tau = -F\cos(\varphi), \\ a_\tau + a\tilde{f}(a)/(2Q_0) = -F\sin(\varphi). \end{cases} \tag{10}$$

These equations do not depend directly on the introduced dissipation function, but on its averaged counterpart. As we have imposed several constraints on the dissipation function, we will briefly consider how

they are related to the averaged dissipation function $\tilde{f}$ before proceeding to the analysis of the model defined by Eqs. (10).

3.1. Remarks about the averaged dissipation function

Evaluation of the averaged dissipation function $\tilde{f}$ associated with a given dissipation function f requires the computation of the integral (8). Explicit relationship between $\tilde{f}$ and f is not available in the general case, but can be readily obtained if f is a low-order polynomial function. The hypothesis of a linear behaviour at low amplitude imposes that the normalised f tends to unity in the small-amplitude limit. The induced time-averaged transparency can be described by introducing in f a quadratic term with a negative coefficient. But such a term will lead to negative dissipation when the argument is far from zero, so that higher-order term(s) should be considered. Odd character of a cubic term will prevent compensation of the negative contribution of the quadratic term. Then a quartic term with a positive coefficient should be chosen:

$$f_{\text{poly}}(a) = 1 + \beta_1 a^2 + \beta_2 a^4. \tag{11}$$

A proper choice of the coefficients values ($\beta_1 < 0$ and $\beta_2 > \beta_1^2/4$) will prevent occurrence of negative dissipation. Neglecting the background dissipation and omitting spatial terms related to the defect location, the temporal averaging procedure yields for the local dissipative function of the defect an expression qualitatively similar to Eq. (11), but with modified coefficients:

$$\tilde{f}(a) = 1 + \tfrac{3}{4}\beta_1 a^2 + \tfrac{5}{8}\beta_2 a^4. \tag{12}$$

This is a polynomial function of the same form as the dissipation function itself. It could be checked that for a positive-definite function f_{poly} the averaged dissipation function $\tilde{f}$ is also non-negative. The background (distributed) dissipation is responsible for a constant positive correction that was neglected above in order to show that the defect is responsible for a positive contribution to the dissipation, whatever is the amplitude. We also remind here that our analysis is performed for the case when the system is excited near one of its resonances. This means that the form of the averaged dissipation function given by Eq. (12) is applicable in a narrow frequency range around a resonance, so that the frequency dependence in $\tilde{f}$ is weak and therefore will be neglected. The above discussed polynomial dissipation function allows for modelling the induced transparency with the net positive dissipation, but diverges far from the origin. Another form of the dissipation function can be proposed which does not diverge:

$$\tilde{f}(a) = r + (1 - r)\exp(-(a/a_c)^{2m}), \tag{13}$$

where a_c is the characteristic strain amplitude for which the transition between two levels of absorption $\tilde{f}(a \ll a_c) \longrightarrow 1$ and $\tilde{f}(a \gg a_c) \longrightarrow r$ takes place, m is an integer that allows to control the width of the transition zone. This model of dissipation function allows one to model the induced transparency if r is chosen between 0 and 1. It will ensure nearly linear behaviour for low ($a \ll a_c$) and high ($a \gg a_c$) amplitudes. There is no explicit relationship to link this averaged dissipation function $\tilde{f}$ to f, but the latter should have qualitatively similar shape.

4. Analysis of the model

We will proceed to the analysis of Eqs. (10) in several steps. The equilibria of the system will be first considered. As the slow variables in system (10) describe oscillations of a mode, a static equilibrium for variables in Eqs. (10) corresponds in fact to a sinusoidal oscillation with a constant amplitude. Thus, finding the equilibria will allow us to simulate resonance curves of the system. At the next step we will consider the stability of these equilibria. It will be shown that the number of the equilibria and their character may change depending on the system parameters leading to bifurcations. We will see that the system may exhibit instabilities that may lead to a switching towards another equilibrium, corresponding to the experimentally observed jumps at the resonance curves, or at certain parameters a limit cycle may exist, corresponding to experimentally observed self-modulation. Finally, special cases of the excitation parameters and dissipation function will be considered.

4.1. Equilibrium states of the system

Eq. (10) are a system of first-order differential equations. Analysis of the behaviour of such equations usually begins with the study of their static equilibria [8], which either attract or repel the system in their vicinity. We consider stationary points $(\bar{a}, \bar{\varphi})$, which by definition satisfy conditions $\dot{\bar{a}}_\tau = \dot{\bar{\varphi}}_\tau = 0$. From Eqs. (10), this leads to

$$(\bar{a}\tilde{f}(\bar{a})/(2Q_0))^2 + \bar{a}^2(\Delta v)^2 = F^2, \tag{14a}$$

$$\tilde{f}(\bar{a})/(2Q_0\Delta v) = \tan(\bar{\varphi}). \tag{14b}$$

This set of equations relates the parameters $\bar{a}$ and $\bar{\varphi}$ describing the stationary response of the system to parameters F and Δv characterising the excitation. For a given excitation, the first equation allows one to obtain the amplitude $\bar{a}$, and once $\bar{a}$ is known, the second equation gives the phase $\bar{\varphi}$. From a geometrical point of view, Eq. (14a) is the equation of a surface in the space $(\Delta v, a, F)$. This surface of stationary amplitudes $\mathscr{F} = F(a, \Delta v)$ is represented in Fig. 5. The dissipation function used to compute this figure (and the following) is of the type of Eq. (13) with parameters $Q_0 = 100$, $a_c = 1$, $r = 1/2$ and $m = 4$. This corresponds to a twofold decrease in dissipation in a narrow amplitude range around the unit amplitude. From Eq. (14a), we see that the intersections between the stationary amplitude surface and the planes in which F is constant are the resonance curves. Some of them are represented in Fig. 5 on the surface itself and in projection on the horizontal plane below. It appears that the surface $\mathscr{F}$ has a local minimum. This point, at amplitude a_2, belongs to a resonance curve associated with a value of F that we call F_1. This critical resonance curve is constituted of the point corresponding to the local minimum at $\Delta v = 0$ (i.e., at the resonance frequency) and the open branch that exists at any driving frequency (see the bold line in Fig. 5, in which other critical resonance curvesare also shown in bold). The surface also has a saddle point at $(\Delta v = 0, a_1, F_2)$ that defines another critical resonance curve. A distinctive feature of this curve is that it crosses itself. There is also a third critical resonance curve that is characterised by the existence of a single point with vertical (i.e., orthogonal to the frequency axis) tangent at each side, whereas neighbouring curves have either two such points or no vertical tangent at all (see the curve labelled F_3 in Fig. 9). These single vertical tangent corresponds to $F = F_3$ and $\Delta v = \pm\Delta v_3$.

These critical values $F_1 < F_2 < F_3$ of F determine four driving strain intervals in which resonance curves demonstrate qualitatively different shapes. The middle column (b) of Fig. 6 shows examples of those curves normalised to the driving strain (that is FRFs). Dashed lines in this figure are linear resonance curves for the quality factors $Q = 100$ and 200. These curves corresponding to linear dissipation should be compared with

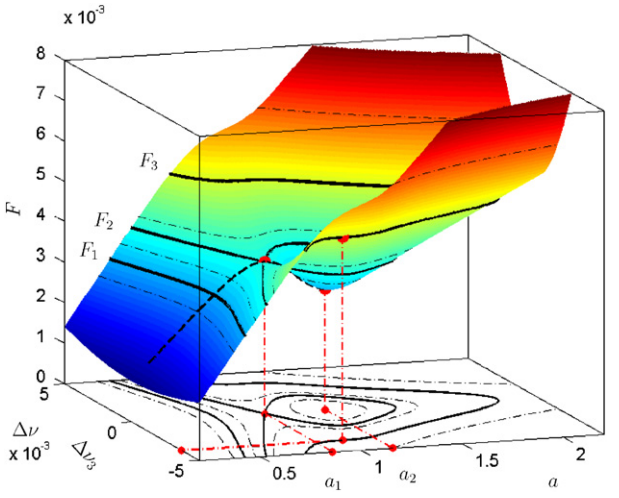

Fig. 5. Stationary amplitudes surface $\mathscr{F}$ with resonance curves (see the solid and dash-dotted lines on the surface and their projections on the frequency–amplitude plane). Resonance curves shown by the solid lines are associated with critical values of F.

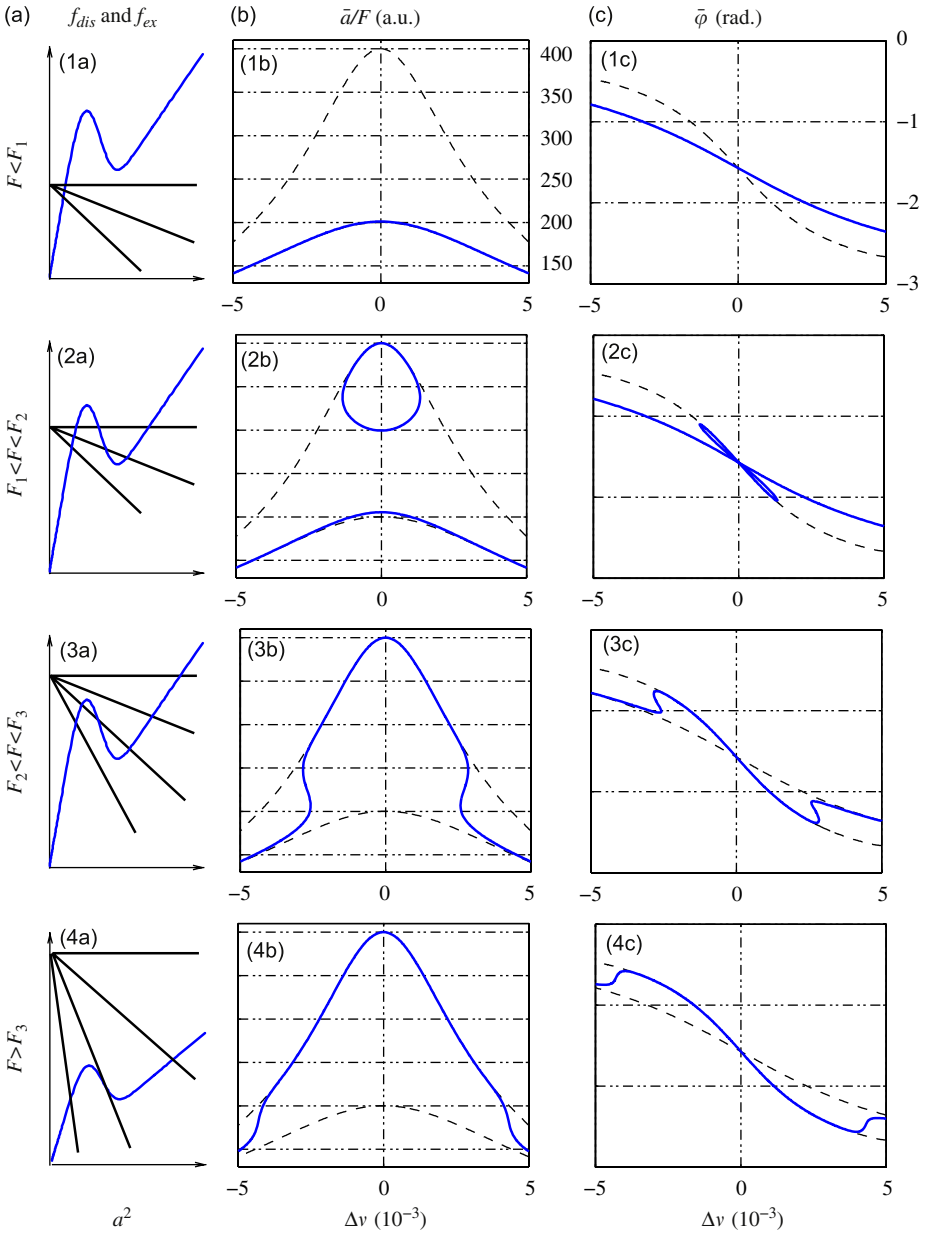

Fig. 6. Schematically shown dependences f_{dis} and f_{ex} as functions of squared amplitudes a for different excitation amplitudes F (column (a)), and the respective amplitude (column (b)) and phase (column (c)) of the resonance curves for a system exhibiting strong induced transparency (scales appear only on top plots). The dashed curves correspond to nearly linear behaviours (at low and high amplitudes).

the solid curves plotted for the nonlinear dissipation function corresponding to $Q = 100$ at low amplitudes and twice higher Q-factor at the high-amplitude limit. At low driving strain ($F < F_1$), the resonance curve is constituted of a single branch whose shape is close to that of the linear curve for $Q = 100$ (see Fig. 6-1b). For the driving strain between F_1 and F_2, another branch appears around resonance frequency (Fig. 6-2b). This new branch is a closed one. Increasing the driving strain over F_2 (Fig. 6-3b) will produce a confluence of the two branches, from which only a single-branch curve remains. This curve is multi-valued as a function of the detuning $\Delta\nu$. For even higher amplitude (greater than F_3), the resonance curve is again single-valued (Fig. 6-4b). Due to the localised amplitude range in which the nonlinear dissipation function significantly

changes its value, the shape of the resonance curves is close to that of the linear-curve shapes except in the range where the oscillation amplitude is close to critical. The right column of Fig. 6 represents the phase for the corresponding nonlinear resonance curves (the dashed lines shown for comparison again correspond to the linear FRFs). The phase is constituted of the same number of branches as its associated resonance curve, and is multi-valued in the same frequency interval. This is a direct consequence of Eq. (14b) which defines a bijection between $\bar{a}$ and $\bar{\varphi}$ at a given $\Delta\nu$.

Now we have described the resonance curves for a particular example of the dissipation function and have seen that it differs from the linear case (where the resonance curves are single-valued and are always of same shape). Obviously, resonance curves cannot be multi-valued if the stationary amplitude surface does not have (at least) a local minimum. Let us consider what constrains on the averaged dissipation function imposes the existence of this local minimum on the stationary amplitude surface F. Since a minimal excitation amplitude F providing a given amplitude $\bar{a}$ corresponds to the exact resonance, $\Delta\nu = 0$, the minimum should be sought along the amplitude direction *at* zero detuning. At $\Delta\nu = 0$ the left-hand side of Eq. (14a) reduces to $(\bar{a}\tilde{f}(\bar{a})/(2Q_0))^2$. For convenience of the further discussion, we introduce notation f_{dis}:

$$f_{\mathrm{dis}}(a) = (a\tilde{f}(a)/(2Q_0))^2. \tag{15}$$

The square root of $f_{\mathrm{dis}}(a)$ correspond to the intersection of the stationary amplitude surface and the plane $\Delta\nu = 0$; it appears partially as a dashed line in Fig. 5. Function f_{dis} is represented in Fig. 7. In the linear case, f_{dis} is monotonic since $\tilde{f}(a) = 1$. Viewed as a function of a^2, it is a growing straight line the slope of which is controlled by the quality factor Q_0. The higher the Q_0 is, the lower is the slope. Occurrence of induced transparency will increase the Q-factor and therefore decrease the slope. Considering an ideal case of induced transparency in which the dissipation possesses two asymptotic values corresponding to low- and high-amplitude regimes, the associated f_{dis} should tend asymptotically to straight lines for the low and high amplitudes. Such lines are shown in the dash-dotted style in Fig. 7. If the induced transparency is too weak, as is illustrated by the dashed curve connecting points A and C, function f_{dis} remains monotonic and has no minima. On the contrary, if the induced transparency is sufficiently pronounced, then function f_{dis} has a local minimum (or minima) as is illustrated by the non-monotonic segment AB on the solid curve in Fig. 7.

We can now formulate that the resonance curves will be multi-valued if in a certain amplitude range the condition $\partial f_{\mathrm{dis}}/\partial a < 0$ is fulfilled. Substitution of Eq. (15) allows one to rewrite this condition in terms of $\tilde{f}$:

$$\tilde{f}'(a) \leqslant -\tilde{f}(a)/a. \tag{16}$$

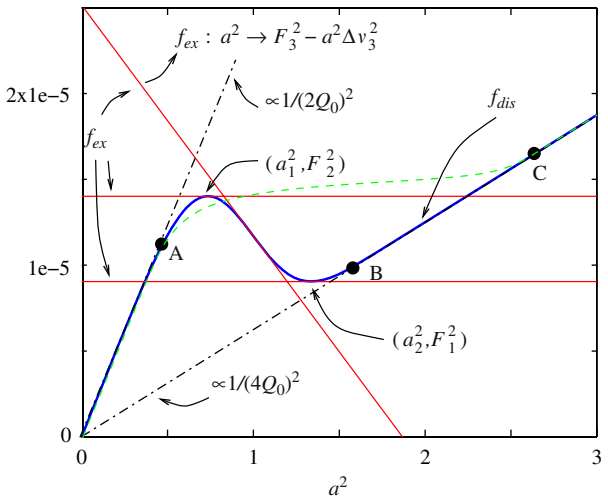

Fig. 7. The dissipation function f_{dis} (thick solid curve) exhibiting strong induced transparency between points A and B shown as functions of a^2. Thin solid lines correspond to three characteristic "excitation lines" f_{ex} corresponding to critical strains F_1, F_2, F_3. The dashed line connecting points A and C has a positive slope everywhere and represents a dissipation function f_{dis} exhibiting weaker induced transparency insufficient to create a local minimum on f_{dis}.

This condition means that function $\tilde{f}$ decreases (locally) faster than $1/a$. If Eq. (16) is satisfied somewhere, some resonance curves of the system will be multi-valued. We assume that Eq. (16) is satisfied in a single interval $[a_1, a_2]$. On the border of that interval, $\partial f_{\mathrm{dis}}/\partial a = 0$ and it follows that a_1 and a_2 are positions of the local maximum and minimum of f_{dis}, respectively (because f_{dis} is increasing outside of $[a_1, a_2]$). Two critical amplitudes a_2 and a_1 are defined and they are reached at resonance for the critical values of normalised strain $F_1^2 = f_{\mathrm{dis}}(a_2)$ and $F_2^2 = f_{\mathrm{dis}}(a_1)$, respectively (as it follows from Eqs. (14a) and (15)).

Introducing the "excitation function" f_{ex}:

$$f_{\mathrm{ex}}(a) = F^2 - a^2 \Delta v^2 \tag{17}$$

allows one to interpret the equilibrium defined by Eq. (14a) as an intersection between functions f_{dis} and f_{ex}. Each particular resonance curve corresponds to the manifold of intersections of f_{dis} with a family of f_{ex} associated with the same value of F. Plotted as a function of a^2, such a family is an ensemble of straight lines passing through the point $(a = 0, F^2)$. The slope of such a line is equal to $-(\Delta v)^2$. All the lines are decreasing, the highest line is the horizontal one obtained at resonance, $\Delta v = 0$. Schematic examples of these lines are given in the left column of Fig. 6 for the different ranges of F. At low amplitudes ($F < F_1$, Fig. 6-1a), the horizontal line f_{ex} (associated with the resonance) passes below the local minimum of f_{dis} and intersects it in a single point. When F is between F_1 and F_2 (Fig. 6-2a), the horizontal f_{ex} passes between the local minimum and maximum of f_{dis}. The resonance curves are therefore multi-valued (three equilibrium amplitudes exist for small enough $(\Delta v)^2$). With increasing $(\Delta v)^2$ the function f_{ex} becomes steeper, and after the threshold slope, at which the line f_{ex} is tangent to f_{dis}, only a single intersection remains. For $F_2 < F < F_3$ (see Fig. 6-3a), the horizontal f_{ex} passes over the local maximum of f_{dis} , so that the resonance is single-valued at resonance $\Delta v = 0$, and two slopes allow for tangency between f_{ex} and f_{dis}.These slopes define two frequency intervals, symmetrical around the resonance, where the resonance curve is multi-valued.

Let us discuss in more detail such a resonance curve, an example of which is given in Fig. 8(a). The dissipation function f_{dis} and several characteristic lines f_{ex} are shown in Fig. 8(b). Let us assume that the driving frequency is swept, and the system moves along the resonance curve starting at point A and passing through the resonance to point A′ (see Fig. 8). Then the oscillation amplitude on the resonance curve and the position of the intersection between f_{dis} and f_{ex} will change continuously everywhere except at point B (where a jump upward to point C occurs) and point E (where a jump downward to point G occurs). The position of the jumps on the Δv-axis are given by the slopes of the respective tangent f_{ex}. Let us consider how these two slopes evolve as F is increased further. From Fig. 8(b), one can see that lines f_{ex} tangent to the local maximum and minimum will both become steeper while the two tangency points (B and E) will approach each other. They will coincide in the inflection point of f_{dis}, for certain excitation amplitude $F = F_3$ and detuning $\Delta v = \pm \Delta v_3$. If the driving strain is higher than F_3, none of the curves f_{ex} is tangent to f_{dis} (see Fig. 6-4a) and only single intersections may occur, so that the resonance curve becomes again single-valued.

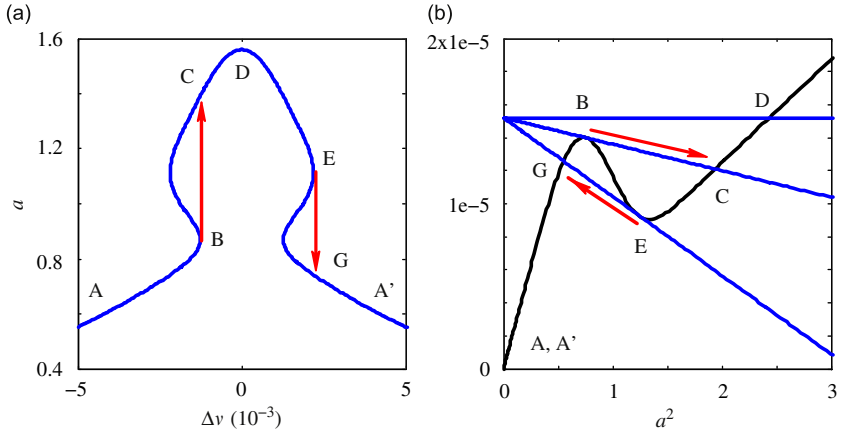

Fig. 8. (a) Resonance curve exhibiting jumps associated with a driving amplitude F in the range between F_2 and F_3. (b) Function f_{dis} (curved line) and functions f_{ex} (straight lines) plotted for the same driving strain at several different detunings.

We have seen therefore that at a given driving amplitude, the resonance curve is multi-valued when there exists f_{ex} tangent to f_{dis}. The slopes of these critical f_{ex} give the frequency intervals where resonance curves are multi-valued.

Let us define the subset J of the stationary amplitude surface $\mathscr{F} = F(a, \Delta v)$, where values F and Δv and the respective a correspond to excitation line f_{ex} that is tangent to function f_{dis}. As lines f_{ex} are decreasing, they can only be tangent to f_{dis} at its decreasing part, that is for amplitudes between a_1 and a_2. Each given $\bar{a} \in [a_1, a_2]$ readily yields the derivative of f_{dis} at this point. On the other hand, by the definition of f_{ex} (Eq. (17)), the slope of the f_{ex} tangent to f_{dis} at that point is equal to the derivative of f_{dis} with respect to a^2. The associated value of F is then obtained by prolonging the tangent up to $a = 0$. The subset $J \subset \mathscr{F}(a, \Delta v)$ is therefore a curve on the surface $\mathscr{F}$ parameterised by the amplitude $\bar{a}$ in the following way:

$$J = \left\{ (\Delta v, F, \bar{a}) \text{ so that} \begin{cases} \bar{a} \in [a_1, a_2] \\ -(\Delta v)^2 = \dfrac{\mathrm{d}}{\mathrm{d}(a^2)} f_{dis}(\bar{a}) = \dfrac{\tilde{f}(\bar{a})[\tilde{f}(\bar{a}) + \bar{a}\tilde{f}'(\bar{a})]}{4Q_0^2} \\ F^2 = f_{dis}(\bar{a}) + (\Delta v)^2 \bar{a}^2 \end{cases} \right\}. \tag{18}$$

The projection of subset J on the $(\Delta v, a)$ plane is represented in Fig. 9 by the boundary, marked J, of the shaded zone. This boundary corresponds to starts of jumps presented in Fig. 8. Further, tangent lines f_{ex}, corresponding to the boundary J in Fig. 9, intersect function f_{dis} at other points (located either at lower or at larger amplitude as is illustrated in Fig. 8: the f_{ex} tangent at point B also has an intersection at point C, the f_{ex} tangent at point E has another intersection at point G). These intersection points correspond to jump arrivals, and the ensemble of all arrival points constitutes in Fig. 9 the outer oval-like boundary shown by the solid line and denoted as J'. The analysis of stability of the equilibrium points of Eqs. (10) in the next section will demonstrate how the sufficiently strong induced transparency can produce switching between stable branches of multi-valued resonance curves, which qualitatively reproduces the experimentally observed jumps visible in Fig. 3.

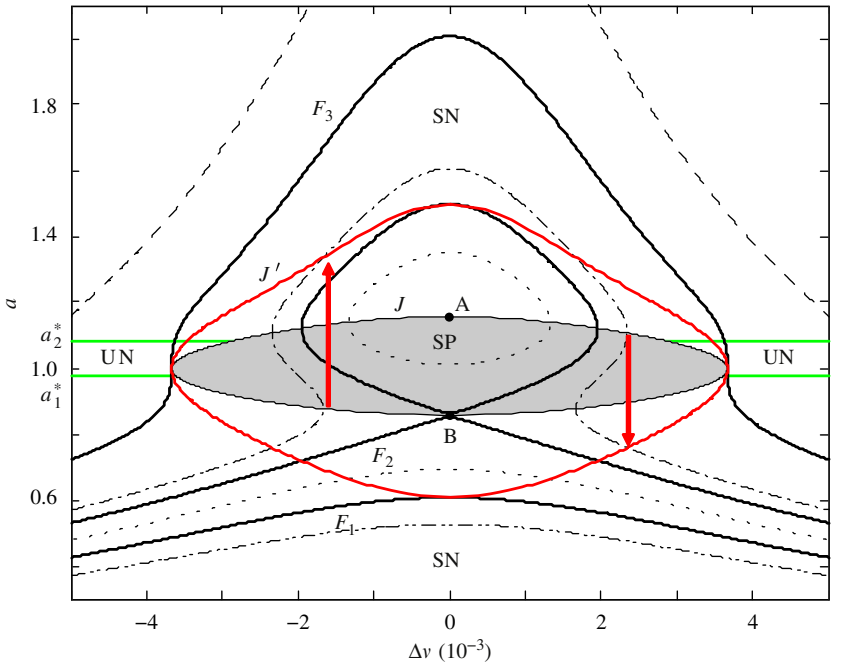

Fig. 9. Resonance curves and instability zones. Notation SN is for stable nodes; UN, unstable nodes; SP, saddle points.

4.2. Stability of the equilibrium states

The stability of the equilibrium points discussed above can be readily studied considering infinitesimal perturbations around an equilibrium $(\bar{a}, \bar{\varphi})$. The perturbed solution $(\bar{a}+\delta a, \bar{\varphi}+\delta\varphi)$ satisfies the linearised equations following from Eqs. (10):

$$\begin{vmatrix} \delta\dot{a} \\ \delta\dot{\varphi} \end{vmatrix} = \begin{bmatrix} -\dfrac{\tilde{f}(\bar{a})+\bar{a}\tilde{f}'(\bar{a})}{2Q_0} & \bar{a}\Delta v \\ -\dfrac{\Delta v}{\bar{a}} & -\dfrac{\tilde{f}(\bar{a})}{2Q_0} \end{bmatrix} \begin{vmatrix} \delta a \\ \delta\varphi \end{vmatrix}. \tag{19}$$

Solution of such a system is a linear combination of $\exp(\lambda_{\pm}t)$ where $\lambda_{\pm}$ are the eigenvalues of matrix in Eq. (19):

$$\lambda_{\pm} = A_1 \pm \sqrt{A_1^2 - A_2}, \tag{20a}$$

$$A_1 = -\frac{2\tilde{f}(\bar{a})+\bar{a}\tilde{f}'(\bar{a})}{4Q_0}, \tag{20b}$$

$$A_2 = \frac{\tilde{f}(\bar{a})[\tilde{f}(\bar{a})+\bar{a}\tilde{f}'(\bar{a})]}{4Q_0^2} + (\Delta v)^2. \tag{20c}$$

If at least one of the characteristic values $\lambda_{\pm}$ has a positive real part, the perturbation will grow with time and the equilibrium will be unstable. We will therefore study the sign of the real part of the eigenvalues as a function of the stationary amplitude $\bar{a}$ and detuning Δv corresponding to the equilibrium points.

Some lines f_{ex} have three intersections with f_{dis} (see Fig. 6). Note that at $a=0$ inequality $f_{ex} > f_{dis}$ is valid, and this inequality is inversed after each intersection point. At the first intersection that occurs in the first increasing part of f_{dis}, line f_{ex} passes below f_{dis}. Then f_{ex} is again above f_{dis} after the second intersection that occurs in the decreasing part of f_{dis}. At that second intersection point, the derivative of f_{ex} is therefore greater than the derivative of f_{dis}, otherwise f_{ex} could not pass over f_{dis} at that point. That means that for such $\bar{a}$, the relationship

$$\frac{\mathrm{d}}{\mathrm{d}(a^2)} f_{ex}(\bar{a}) = -(\Delta v)^2 > \frac{\mathrm{d}}{\mathrm{d}(a^2)} f_{dis}(\bar{a})$$

is satisfied. It can be verified from Eq. (20c) that $A_2 < 0$ if this condition is satisfied. We also can see from Eq. (18) that on curve J corresponding to equality

$$-(\Delta v)^2 = \frac{\mathrm{d}}{\mathrm{d}(a^2)} f_{dis}(\bar{a}),$$

value $A_2 = 0$. The zone where $A_2 < 0$ corresponds to the interior of J, the latter being the locus of a saddle-node bifurcation. In the interior of J, the square root in Eq. (20a) is greater in the absolute value than A_1, so that the two eigenvalues are real and of opposite signs, which corresponds to unstable equilibrium points of the saddle-type (SP). This interior zone of curve J is shaded in Fig. 9.

Outside of this zone inequality $A_2 > 0$ is valid. The argument of the square root in Eq. (20a) can be either positive or negative, but in both cases the signs of the real parts of $\lambda_{\pm}$ are determined by the sign of A_1. In the linear case, A_1 reduces to $-1/(2Q_0)$ which is negative, all equilibria are stable (and neither the SP zone inside J nor boundary J itself do exist). Such equilibrium points whose eigenvalues have real parts of the same sign are nodes (note that often term focus is used for nodes having the imaginary parts of the eigenvalues). The latter distinction does not influence stability, and we will denote both the types as nodes. Outside of zone J (if it exists due to nonlinear dissipation) or everywhere (if J does not exist), equilibrium points are nodes that are stable if $A_1 < 0$ (SN: stable node). This readily gives a condition for existence of a second instability zone:

points outside of J so that $A_1>0$ are unstable nodes (UN: unstable node). The latter in accordance with Eq. (20c) requires the condition

$$\tilde{f}'(a) \leqslant -2\tilde{f}(a)/a. \tag{21}$$

Inequality (21) is similar to condition (16) that requires sufficiently rapid decrease of the positive-averaged dissipation function $\tilde{f}$. However, Eq. (21) requires the derivative of $\tilde{f}$ to be even more negative. This new condition can therefore be satisfied only at some parts of interval $[a_1, a_2]$ introduced for condition (16). The averaged dissipation function used for simulations admits only one such interval $[a_1^*, a_2^*]$. Points with equilibrium amplitude $\bar{a} \in [a_1^*, a_2^*]$ located outside zone J are unstable nodes. They are denoted as the UN-zone in Fig. 9 localised between the horizontal straight lines corresponding to amplitudes a_1^* and a_2^*.

After classification of the resonance curve types (single- or multi-valued) and the equilibrium types (SP, UN or SN), possible regimes of the considered system can be also readily classified. Being attracted by a stable point, the system will simply remain there. Near unstable equilibria the system will be repelled and could then be attracted by a stable fixed point if the latter exists. For multiple equilibria, their number and nature, as well as the initial conditions will determine the system behaviour. For instance, we can recover the jumping behaviour presented in Fig. 8. On a resonance curve associated with values of F between F_2 and F_3, like the dash-dotted curve in Fig. 9, all points are stable except of those inside of boundary J. Jumps *therefore has to* start at points where the resonance curve crosses boundary J of the shaded zone and must arrive at boundary J' as is illustrated in Fig. 9.

Furthermore, in the absence of strong perturbation, the jumps cannot take place in a zone inside of J' but outside of J, because even if multiple equilibria exist, the initial equilibrium is stable in such a case.

Let us now consider resonance curves for smaller excitation amplitudes F between F_1 and F_2. Such resonance curves are composed of a closed loop and an open branch. It can be seen in Fig. 9 (dotted curves) that the open branch is stable, as well as the upper part of the closed branch. This implies that an experimental acquisition of such a curve will only give its stable part. The lower part of the closed loop is not observable because of its instability, and the upper part can only be retrieved if the system switches to the upper branch in the case of a strong perturbation sufficient to bring the system in the attraction zone of the upper branch.

Attraction zones for different equilibria can be conveniently represented on the phase plane (a, φ) corresponding to the discussed system. In the case of a single and stable equilibrium, all trajectories on the phase plane will tend to this single attractor. If multiple attractors coexist, for instance, one saddle point and two stable nodes (which is the case for most of the excitation parameters leading to multiple equilibria), then the stable nodes constitute two attractors and the saddle point belongs to the frontier between their basins of attraction.

Behaviour of dynamical systems such as Eqs. (10) is often characterised via vector fields of tangents to trajectories of the representation point on the phase plane. Starting from a particular point (a, φ), the system (10) can be rewritten in order to give directly the time derivative of the variables (and thus to determine tangents to the trajectories on (a, φ)-plane):

$$\begin{cases} \dot{\varphi} = -F\cos(\varphi)/a - \Delta\nu, \\ \dot{a} = -F\sin(\varphi) - a\tilde{f}(a)/(2Q_0). \end{cases} \tag{22}$$

Using these equations, equilibrium points can be interpreted as intersections between the curves defined by the right-hand sides of Eqs. (22) at $\dot{a}=0$ and $\dot{\varphi}=0$. These curves are shown by thin solid lines in the right part of Fig. 10 (together with the tangent vector fields), and their intersections represent multiple equilibria for resonance curves with one branch (top plot) and two branches (bottom). The left part of Fig. 10 shows the respective resonance curves. The vector fields in the right plots give an instructive representation on the basins of attraction for the equilibrium points. One may see that each point with amplitude a lower or equal to the amplitude of the lower equilibrium belongs to its basin of attraction (whatever is the phase variable φ), so that even arbitrary strong phase perturbations will not switch the system towards the other equilibrium. Such switching requires sufficiently strong amplitude perturbation accompanied by a proper phase condition. The low-amplitude equilibrium is therefore highly stable and the closed branch of the resonance curve would be hardly observable in experiment.

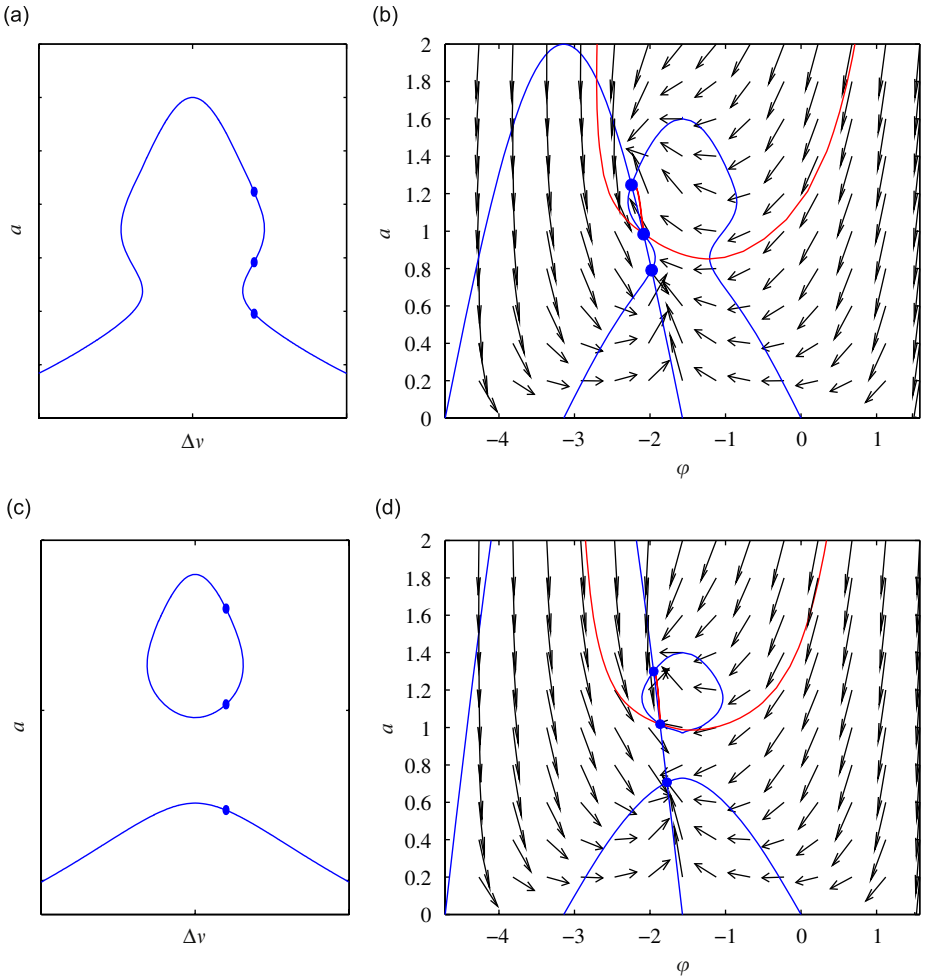

Fig. 10. Phase field for given excitation parameters (b,d) and the respective stationary amplitudes shown as bullet points on the resonance curve for the same parameters (a,c). The thin solid curves on the right plots correspond to stationary values of either a or φ. Thick solid curves correspond to trajectories almost coinciding with the boundaries of the attraction basins of those equilibrium points.

4.3. Limit cycle and self-modulation

So far, we discussed only resonance curves with a saddle point and stable nodes. Let us now consider a resonance curve that crosses only the SN- and UN-zones, but not the SP-zone. This case corresponds to the driving amplitudes higher than F_3, for which the resonance curves are single-valued. Since even in the unstable UN-zone the system does not diverge, this suggests the existence of a limit cycle corresponding to a non-stationary (oscillating) solution. This conclusion is also supported by the existence of non-zero imaginary part of eigenvalues (20a) in this parameter range, which may be used for a rough estimation of the expected oscillation frequency.

However, such estimates are based on the linearised system (19) assuming infinitesimal oscillation amplitude, whereas experimental observations (see, e.g., Fig. 4) revealed the cases of rather pronounced modulation. Description of such regimes in the framework of the small perturbation approach was insufficient, so that numerical simulations based on nonlinear equations (10) were performed.

The numerical simulations showed that the threshold conditions (for jumps or for the non-stationary regimes of self-modulation) are well predicted by the perturbation theory. Figure 11 demonstrates typical examples of the self-modulation regimes. The upper part of the figure shows parts of resonance curves with indicated instability zones. Three resonance curves that cross the UN-zone are presented. Particular points

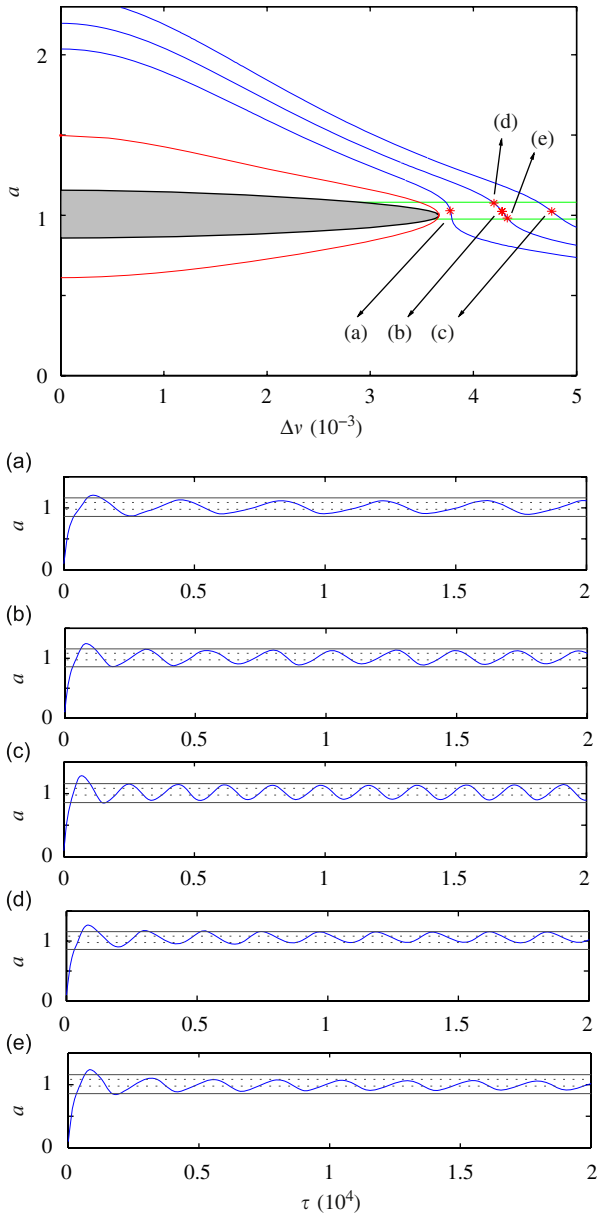

Fig. 11. Simulated temporal amplitude behaviour for various excitation parameters in the modulation instability zone.

that are labelled from (a) to (e) correspond to various driving conditions. Temporal signals associated with those excitations are represented in the lower part of Fig. 11. The simulations (a), (b) and (c) correspond to identical stationary amplitudes. They are obtained by proper simultaneous increase in the parameters F and Δv. Simulations (d), (b) and (e) are obtained at the same driving level, but with increasing detuning Δv from the resonance. It can be seen from (a), (b) and (c) that the period of the limit cycle decreases as the driving frequency gets away from resonance. It was also observed that amplitude excursions in the self-modulation regimes could get beyond the range $[a_1^*, a_2^*]$ but remain between critical amplitudes a_1 and a_2 (see, respectively, dashed horizontal lines in Fig. 11 and the wider separated solid lines). In accordance with experimental observations, the numerical simulations based on Eqs. (10) and analytically found imaginary parts of eigenvalues (20a) of linearised system (19) consistently predicted that the frequency of the self-modulation may range from near-zero values to values of the order of the resonance curve width.

We have found a new mechanism that leads to bifurcations associated with bistability and self-modulation. It differs from mechanisms of self-modulation earlier discussed in nonlinear acoustics owing to its purely nonlinear-dissipative character with strictly positive dissipation. This mechanism suggests that the system exhibits sufficiently strong induced transparency. It is the steepness of the dissipation diminishing with increasing excitation amplitude which is important, rather than the amount of the dissipation decrease. For instance, such phenomena should be expected in systems with dissipation that decrease in a stepwise fashion.

4.4. Special cases and more general dissipation functions

In addition to classification of main dynamical regimes considered above, let us briefly consider some mixed types on the system behaviour. So far, based on the experimental data we considered the nonlinearity of the system as purely dissipative. The analysis performed above has confirmed that the modulational instability and the bistability of resonance curves can occur for the dissipation nonlinearity alone. In the absence of nonlinear elasticity, the right and left parts of resonance curves are symmetrical, although positions and magnitudes of jumps due to the induced transparency are essentially asymmetric at the left- and right-halves of the resonance curve. The reason for this asymmetry is elucidated in the schematic Fig. 8, where the right jump downward is essentially weaker and is more distant from the resonance maximum than the left jump upward. On the scale of the frequency sweep presented in the experimental Fig. 2, only one (closest to the resonance) jump downward is visible, its magnitude being essentially smaller than that of its upward counterpart located at the left part of the resonance curve. It can be noted that together with the pronounced induced transparency, a slight shift of the resonance frequency can be distinguished for FRF-curves in Fig. 2 indicating a weak odd-type elastic nonlinearity. However, main features of the considered nonlinear-dissipative mechanism should remain in the presence of accompanying nonlinear elasticity, although the latter may induce more pronounced asymmetry between the system behaviours for frequencies below and above the resonance frequency. For instance, it is well known that cubic elastic non-linearity leads to simultaneous shift and bending of resonance curves (Duffing oscillator [14]), which may induce jumps (bistability) only at one (concaved) side of the resonance curve. Thus additional odd-type elastic nonlinearity, depending on its sign, may either enhance or reduce the asymmetry of the jumps, which is intrinsic to the purely dissipative nonlinearity.

Concerning the analysis of stability of the equilibrium points and their graphical interpretation as intersections of the dissipation curve f_{dis} and the "excitation line" f_{ex} (like it is illustrated in Fig. 7), the main conclusions should also keep their validity in the presence of an additional odd-type nonlinear elasticity. The latter should make the frequency detuning $\Delta\nu$ dependent of the amplitude, $\Delta\nu = \Delta\nu(a)$, which in its turn,

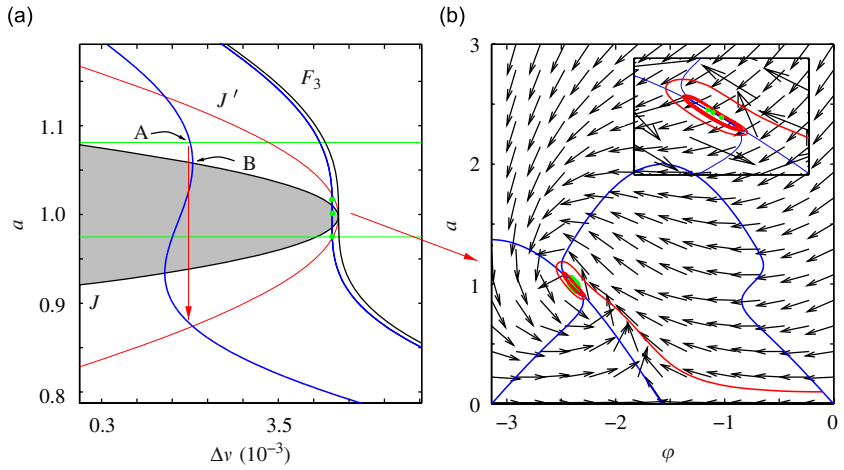

Fig. 12. (a) Some particular cases which are likely to take place where instability zones meet. Vertical arrow points a jump that occurs before what should be expected without stability analysis. The other arrow points out the behaviour of the system with three unstable equilibria. (b) displays a trajectory in such a case; the inset shows the trajectory cycling around the fixed points.

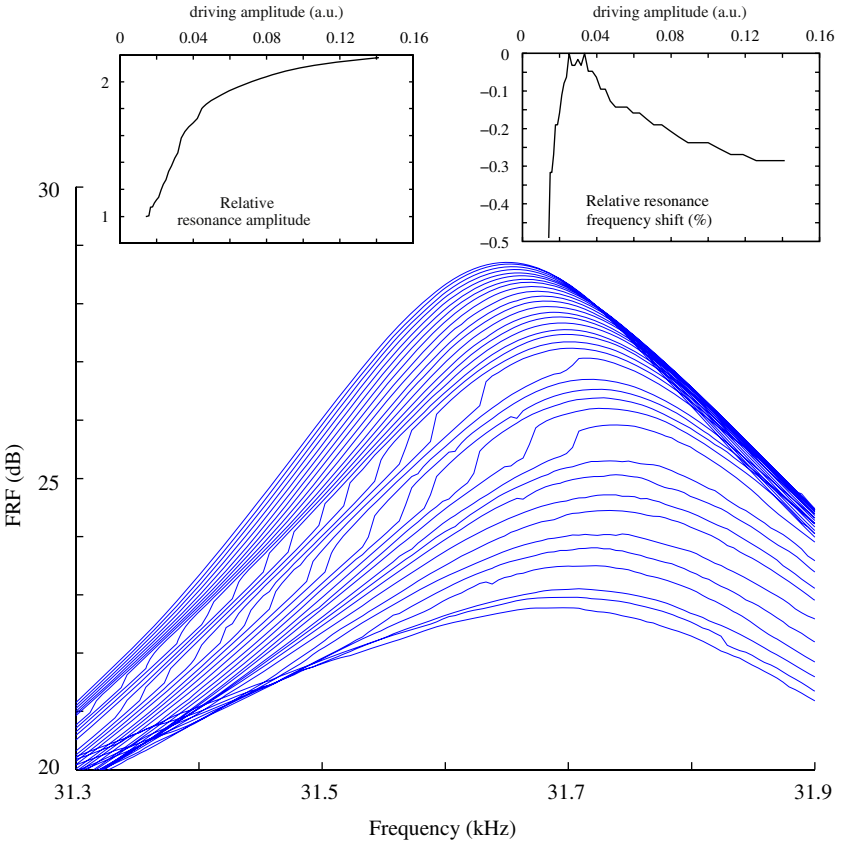

Fig. 13. Successive FRF-curves for the fourth mode obtained with 0.5 dB steps in excitation amplitude. Insets show the relative evolution of resonance amplitude (left) and resonance frequency normalised to resonance width (right) with driving amplitude.

according to Eq. (17), should transform straight lines f_{ex} (when considered as functions of a^2) into bended curves. Nevertheless, the graphical interpretation of the equilibrium points as intersections of f_{dis} and f_{ex} and conclusions concerning the associated jumps (as shown in Fig. 8) qualitatively remain the same.

If the elastic nonlinearity is sufficiently strong, then the resonance curve associated with F_2 (see Fig. 9) can be bent so strongly that it becomes multi-valued only at one side (for example, only below the resonance maximum). In such a case, the jump could only be observed at one side of the resonance curve. Fig. 13, corresponding to the FRF-functions obtained for the fourth resonance of the sample, demonstrates such a mixed case of coexisting dissipative and odd-type elastic nonlinearities. The latter causes quite a pronounced shift and bending of the resonance curves, which results in the presence of jumps only at one side of the resonance.

Another peculiar feature visible in Fig. 13 is an essentially uneven "strength" of the induced transparency. Namely, amplitude ranges, in which the system exhibits the induced transparency sufficient to cause jumps, are separated by a range where the induced transparency is weaker and is unable to induce jumps. Therefore, the condition of the self-modulational instability can also be satisfied in several amplitude ranges, between which the induced transparency is not sufficiently strong to induce the self-modulation. Correspondingly, at the stability maps, instead of only one amplitude range corresponding to modulational instability (like in Fig. 9), several MI-ranges may occur. These zones may be crossed by the system several times when varying either the excitation frequency of the excitation amplitude. Thus during monotonic variation of those parameters, the self-modulation may appear and disappear several times. Physically, different types of the induced transparency are associated with more or less complex structure of the interfaces in the artificial defect. By slightly varying the insert position in the saw-cut, our set-up allowed us to obtain different properties of the system: almost pure dissipative nonlinearity (as in Fig. 2) and the mixed nonlinear-dissipative/nonlinear elastic

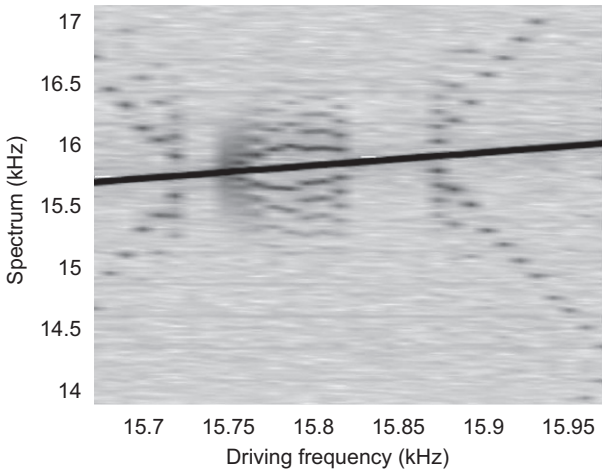

Fig. 14. Experimental spectra around the driving frequency of the vibrations of the system excited with varying frequency close to the second resonance. The main line represents the driving frequency, other components are related to side-lobes of modulation and present a non-trivial behaviour.

behaviour (like in Fig. 13) including the cases of multiple zones of the modulational instability. An example of such multiple appearance/disappearance of the MI is shown in Fig. 14, which demonstrates that characteristics of the modulation can depend on the driving parameters in a non-trivial manner. Three frequency intervals are visible in which the modulation is active. In the two extreme intervals, the modulation frequency demonstrates a linear dependence on the driving frequency and tend to zero frequency where modulation vanishes. Between these intervals is another frequency interval in which modulation happens. The modulation frequency dependence is not linear with the driving frequency in that interval.

Note that even for a relatively simple form of the nonlinear dissipation function f_{dis} with a single interval $[a_1^*, a_2^*]$ of the modulational instability, besides the equilibrium variants discussed in the previous section, other regimes are possible, albeit for very limited ranges of parameters. Namely, near the inflection point of a monotonically decreasing function f_{dis} for a nearly tangent "excitation line" f_{ex} three intersections (equilibriums) may occur, so that all three points belong to the amplitude range $[a_1^*, a_2^*]$ corresponding to MI and all three are unstable. Such a situation may happen in a narrow vicinity of the left and right vertexes of the oval-like curves encountering the zones of jumps at the resonance curves (see Fig. 9). In more detail, the behaviour of the system in such special cases is elucidated in Fig. 12 demonstrating two examples. The figure presents the instability zones, one resonance curve associated to F_3 and two special resonance curves crossing the very edge of the oval-like zones of jumps. It should be reminded here that the boundary of the inner (grey colour) oval-like zone corresponds to tangent points of the "excitation line" f_{ex} at the negative-slope part of function f_{dis}, which corresponds to point of vertical slope at the resonance curves. The left resonance curve in Fig. 12 is a multi-valued one on which we should expect the occurrence of jumps. Without the stability analysis, the jump down would have been expected to start from point marked B, where the resonance curve slope is vertical. However, actually the jump may start earlier at point A, because the whole segment AB of the curve is already unstable since it belongs to the UN-zone located in the region $[a_1^*, a_2^*]$ shown by the horizontal line in Fig. 12. This earlier jump is associated with the combination of the unstable node, the saddle point and the stable node corresponding to the intersections of the resonance curve and the vertical line started at point A.

The other special resonance curve shown in Fig. 12 corresponds to values of F slightly below F_3. This resonance curve is multi-valued, and in a very small detuning interval close to $\Delta\nu_3$ all its three values for a given frequency correspond to unstable equilibrium points within the range $[a_1^*, a_2^*]$: one point is a saddle inside J, and the two others, outside of J, are yet located between a_1^* and a_2^* (and are therefore unstable nodes). The right part of Fig. 12 shows a trajectory in the phase space corresponding to the latter case. The trajectory evolves in the direction of the three fixed points and finally follows a limit cycle encountering all three points as

is shown in the inset in a larger scale. For increasing excitation amplitude at the point corresponding to F_3 and $\Delta\nu_3$ (intersection of the resonance curve F_3 with J) on the left plot in Fig. 12 this triple equilibrium degenerates into one unstable node encountered by the limit cycle. Thus, in the near vicinity of $(F_3, \Delta\nu_3)$ the limit cycle can encounter either one or three equilibrium points. For these special cases only the thresholds are slightly shifted, which does not result in a qualitatively new behaviour of the system.

5. Conclusion

The experiments performed have demonstrated the possibility of bistability and self-modulation in systems with microstructure-induced nonlinearity. The developed model allows one to reproduce the main features of the experiments by introducing in the system purely dissipative nonlinearity. It was proven that the resonance curves could be multi-valued if the nonlinear dissipation manifests itself in the form of strong enough induced transparency. This multi-valued character allows the observation of jumps on the resonance curves. Furthermore, it is demonstrated that even stronger induced transparency can lead to another instability mechanism. Namely, the stationary amplitude can become unstable and the system can be attracted by a limit cycle, which corresponds to the experimentally observed self-modulation regime. This constitutes the first experimental observation and theoretical elucidation of such a dissipative behaviour. From the mathematical analysis of stability of the linearised system, we formulated conditions (that is properties of the nonlinear dissipation and the driving parameters) for which these regimes can be observed. Since the fully developed self-modulation regime corresponds to essentially nonlinear non-stationary solutions, numerical simulations based on the non-stationary nonlinear equations were performed for comparison with the experiments. It is shown that main features of the self-modulation and bistability similar to experiments can be obtained by appropriately tuning the dissipation function [15]. The details of the dissipation function cannot be reconstructed from the experimental data on the equilibrium points observable only for stable parts of the resonance curves. The relation of the self-modulation parameters and the dissipation function is rather complex, so that the inverse problem, that is the reconstruction of the detailed shape of the dissipation function from the self-modulation features, probably has no unique solution and requires deeper theoretical developments. For instance, modelling of the experimentally observed examples of self-modulation with multiple temporal scales also requires further studies.

Physically, the nonlinearity of the experimental sample is connected to the presence of the insert placed in the saw-cut. The insert adds interfaces with multiple contacts between them. Several mechanisms can contribute to the observed transparency. For instance, contacts are known to exhibit efficient dissipation mechanisms such as stick-slip (due to friction) and thermoelastic dissipation. Those effects are known to be amplitude-dependent [7,13], and it has already been proved that their contribution to the overall dissipation can be important [16]. The strong induced transparency may be caused by the inherent amplitude-dependent character of these mechanisms at each contact and by a variation in the number of the contacts with varying excitation amplitude. The self-modulation regime may present some similarity with another type of thermoelastic instability of contacts described in Ref. [12, p. 391]. For a sliding contact with varying loading, the friction forces (and the associated dissipation) will be greater for maximal loads. These local regions will expand due to thermoelastic effect, which may result either in creation or disappearance of contacts. When such a contact is broken, the dissipation due to sliding friction stops and the temperature locally diminishes, so that the contact restores again. The thermoelastic instability of sliding contacts therefore implies periodic opening and closing of some micro-contacts. In our experiments, there is no heat source due to continuous sliding. But the acoustic excitation may generate the heat source at contacts, some of which may open after a certain time due to strains caused by thermal expansion. Opening of such contacts should decrease the acoustic energy dissipation, which corresponds to the induced transparency of the system. Due to heat diffusion the contact can relax to the initial closed state, so that the process can repeat periodically and can manifest itself as the experimentally observed slow modulation. Alternatively, the asymmetrical stiffness of contacts leads to an influence of the vibrations on the average state of the contacts. This provides another opportunity to modulate the characteristics/number of the contacts, and therefore another mechanism likely to contribute to the self-transparency.

These results extend the list of manifestations of the "non-classical" acoustic nonlinearity and provide better insight in the physics of nonlinear interaction of elastic waves with crack-like defects, which is the background of nonlinear-acoustic method for crack diagnostics.

Acknowledgements

The study was supported in parts by a DGA bourse (L.F.), a French-Russian program PECO-NEI 19118 and RFBR Grant nos. 05-02-17 355 and 06-02-72550-CNRSL (V.Z.).

References

[1] L. Landau, E. Lifshitz, *Theory of Elasticity*, Pergamon Press, Oxford, 1959.
[2] K.R. McCall, R.A. Guyer, G.N. Boitnott, Hysteresis, discrete memory, and nonlinear wave propagation in rock: a new paradigm, *Physical Review Letters* 74 (17) (1995) 3491–3494.
[3] Y. Zheng, R.G. Maev, I.Yu. Solodov, Nonlinear acoustic application for material characterization: a review, *Canadian Journal of Physics* 77 (1999) 927–967.
[4] L. Ostrovsky, P. Johnson, Dynamic nonlinear elasticity in geomaterials, *Rivista del Nuovo Cimento* 24 (2001) 1–46.
[5] V. Zaitsev, V. Gusev, B. Castagnède, The Luxemburg–Gorky effect retooled for elastic waves: a mechanism and experimental evidence, *Physical Review Letters* 89 (10) (2002) 105502.
[6] V. Zaitsev, L. Matveev, Strain-amplitude dependent dissipation in linearly dissipative and nonlinear elastic microinhomogeneous media, *Russian Geolology and Geophysics* 47 (5) (2006) 694–709.
[7] L. Fillinger, V.Yu. Zaitsev, V. Gusev, B. Castagnède, Nonlinear relaxational absorption/transparency for acoustic waves due to thermoelastic effect, *Acustica Acta united with Acustica* 92 (2006) 24–34.
[8] R.C. Hilborn, *Chaos and Nonlinear Dynamics*, Oxford University Press, Oxford, 2000.
[9] A. Moussatov, B. Castagnède, V. Gusev, Frequency up-conversion and frequency down-conversion of acoustic waves in cracked materials, *Physical Letters A* 301 (2002) 281–290.
[10] K. Pfeiderer, I. Solodov, J. Wackerl, G. Busse, Nonlinear self-modulation and subharmonic acoustic spectroscopy for damage detection and location, *Applied Physics Letters* 84 (2004) 5386–5388.
[11] J. Guckenheimer, P. Holmes, *Nonlinear Oscillations, Dynamical Systems, and Bifurcation of Vector Fields*, Springer, Berlin, 1983.
[12] K.L. Johnson, *Contact Mechanics*, Cambridge University Press, Cambridge, 1985.
[13] R.D. Mindlin, H. Deresiewicz, Elastic spheres in contact under varying oblique forces, *Journal of Applied Mechanics* (1953) 327–344.
[14] A.H. Nayfeh, D.T. Mook, *Nonlinear Oscillations*, Wiley Classic Library, 1995.
[15] V. Zaitsev, L. Fillinger, V. Gusev, V. Castagnède, Self-modulation phenomena at a single crack-like defect: obersvation and modeling, *Proceedings of Forum Acusticum 2005*, Budapest, Hungary, August 29–September 2, 2005, pp. 1379–1384;
L. Fillinger, V.Yu. Zaitsev, V. Gusev, B. Castagnède, Wave self-modulation in an acoustic resonator due to self-induced transparency, *Europhysics Letters* 76 (2) (2006) 229–235.
[16] V.Yu. Zaitsev, V. Gusev, B. Castagnède, Thermoelastic mechanism for logarithmic slow dynamics and memory in elastic wave interaction with individual cracks, *Physical Review Letters* 90 (7) (2003) 075501.